

Movie-maps of low-latitude magnetic storm disturbance

Jeffrey J. Love¹ and Jennifer L. Gannon¹

Received 14 August 2009; revised 10 December 2009; accepted 6 February 2010; published 5 June 2010.

[1] We present 29 movie-maps of low-latitude horizontal-intensity magnetic disturbance for the years 1999–2006: 28 recording magnetic storms and 1 magnetically quiescent period. The movie-maps are derived from magnetic vector time series data collected at up to 25 ground-based observatories. Using a technique similar to that used in the calculation of Dst , a quiet time baseline is subtracted from the time series from each observatory. The remaining disturbance time series are shown in a polar coordinate system that accommodates both Earth rotation and the universal time dependence of magnetospheric disturbance. Each magnetic storm recorded in the movie-maps is different. While some standard interpretations about the storm time equatorial ring current appear to apply to certain moments and certain phases of some storms, the movie-maps also show substantial variety in the local time distribution of low-latitude magnetic disturbance, especially during storm commencements and storm main phases. All movie-maps are available at the U.S. Geological Survey Geomagnetism Program Web site (<http://geomag.usgs.gov>).

Citation: Love, J. J., and J. L. Gannon (2010), Movie-maps of low-latitude magnetic storm disturbance, *Space Weather*, 8, S06001, doi:10.1029/2009SW000518.

1. Introduction

[2] Magnetic field data produced by ground-based magnetic observatories are rich with information. The data are useful for a wide variety of applications, including measuring the intensity of magnetic storms and mapping their time-dependent evolution. Of particular importance for monitoring space weather conditions is the storm time disturbance index Dst , defined by a weighted average of disturbance data from a sparse longitudinal distribution of 4 low-latitude magnetic observatories [Sugiura, 1964; Sugiura and Kamei, 1991]. Dst is usually interpreted in terms of the energy of an equivalent magnetospheric ring current that flows westward in the equatorial plane [Singer, 1957; Dessler and Parker, 1959; Sckopke, 1966], and as such, the index is a fundamental measure of the intensity of a magnetic storm. However, Dst does not, in any way, measure the local time shape of low-latitude magnetic disturbance. But with the present operation of numerous low-latitude observatories, each producing high-quality magnetometer data, we can make maps of the local time functional dependence of storm time disturbance. With these maps we can obtain a better understanding of the formation and decay of the storm time ring current, and, more generally, illuminate the complex storm time coupling

that exists between the ionosphere, the magnetosphere, and the interplanetary magnetic field. All of this can help in mitigating the hazardous impacts that magnetic storms can have on the activities and infrastructure of our modern, technologically based society [e.g., Baker *et al.*, 2009].

[3] A schematic depiction of a typical storm time Dst time series is shown in Figure 1. Storms often commence with a “sudden impulse,” an abrupt and positive increase in Dst . Chapman and Ferraro [1930] hypothesized that this is due to a pressure impulse in the solar wind that compresses the dayside of the magnetosphere, bringing the magnetopause closer to the Earth’s surface and intensifying its eastward directed electric currents. This produces a positive perturbation in the horizontal magnetic field as measured at low-latitude magnetic observatories and, correspondingly, a positive perturbation in Dst . If the enhancement of solar wind pressure persists for a noticeable duration of time, then the initial impulse leads into an “initial phase,” where Dst is positive and relatively steady. Initial phases can last for only a few minutes or they can persist for several hours [e.g., Akasofu and Chapman, 1972].

[4] While sudden impulses and initial phases are important geomagnetic phenomena, in the modern vocabulary of space weather, magnetic storms are usually defined in terms of a “main phase” and subsequent “recovery” [e.g., Gonzalez *et al.*, 1994]. As the energy of the ring current intensifies, Dst becomes negative relative to its zero-value

¹U.S. Geological Survey, Denver, Colorado, USA.

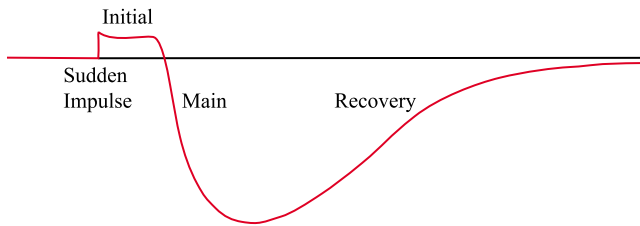


Figure 1. Schematic representation of a typical Dst time series having four different and distinct phases.

quiet time baseline. This energy is correlated with the orientation of the interplanetary magnetic field [Rostoker and Fälthammar, 1967; Russell *et al.*, 1974]. When it is southward directed, dayside magnetic reconnection is facilitated [Dungey, 1961; Cowley, 1995]. This opens the magnetosphere to interplanetary space, driving magnetospheric convection [e.g., Kennel, 1995]. The process can be highly dynamic, with occasional substorm collapse of the tail current [McPherron, 1997; Kamide *et al.*, 1998b], the injection of ions into the ring current from the tail [Kozyra and Liemohn, 2003], and the upflow of ions from the ionosphere [Daglis *et al.*, 1999].

[5] During storm main phase, low-latitude magnetic disturbance is often observed to be asymmetric in local time. This is interpreted in terms of partial ring currents [e.g., Fukushima and Kamide, 1973], with part of the ring current making a complete circuit around the Earth, part connected onto field-aligned currents with circuit closure through the ionosphere, and part simply flowing from the magnetotail into the inner magnetosphere and then out to the magnetopause. With a turning of the interplanetary magnetic field northward, ring current energy injection is damped, and with ion-electron charge recombination the ring current decays. During storm recovery, low-latitude magnetic disturbance is typically relatively symmetric in local time, and, finally, Dst slowly returns to its near-zero quiet time baseline.

[6] To enable quantitative analysis of storm time magnetic disturbance, and to facilitate comparisons of observatory data with theories, numerical simulations, and satellite data, we seek to map time-dependent low-latitude magnetic disturbance in a magnetospheric reference frame. Of course, geomagnetic observatories produce time series from fixed geographic sites. We bridge this reference frame difference by adopting a plotting convention that accommodates both Earth rotation and the universal time dependence of magnetospheric disturbance. Our work here is inspired by that of others who investigated the phase relationship between universal and local time dependence of magnetic disturbance [Zaitzev and Boström, 1971; Clauer and McPherron, 1974; Clauer *et al.*, 2003; Søraas *et al.*, 2006]. But rather than display results in static form, as would be normal in a journal article, we exploit the relative ease with which dynamic images can now be constructed

and viewed on computers; our results are presented as movie-maps.

2. Observatory Data

[7] In making our movie-maps, minute-mean magnetometer data from a longitudinal necklace of low-latitude observatories are used. Magnetic observatories are specially designed and carefully operated facilities that provide accurate data over long periods of time [e.g., Jankowski and Sucksdorff, 1996; Love, 2008]. Since 1991 the INTERMAGNET consortium has set standards for observatory operation, and the organization has validated and published 1 min resolution digital data from the observatories of member institutes [e.g., Kerridge, 2001; Rasson, 2007]. For each INTERMAGNET observatory, raw 1 min variational data, usually collected from a fluxgate sensor, are combined through data processing with calibration measurements to produce magnetic vector time series having long-term stability and accuracy, usually much better than 5 nT. The data are reported on the INTERMAGNET Web site as definitive data in either Cartesian components (X north, Y east, Z down) or horizontal polar components (H horizontal intensity, D declination, Z down). Conversion between the two coordinate systems is simple. Time stamps have been consistently assigned on the top of the universal time minute (HR:MN:SC, 00:00:00, 00:01:00, etc.).

[8] Following Sugiura [1964], we choose observatories (Table 1 and Figure 2) whose data can be reasonably interpreted in terms of an equatorial ring current. The chosen observatories must not be located at latitudes that are so high (low) that they have storm time disturbance fields that are dominated by the auroral zone (equatorial) electrojet; the highest (lowest) magnetic latitude observatory considered here is San Pablo-Toledo (SPT) (Alibag (ABG)) at 42.78°N (10.19°N). Of course, there do not exist distinct latitude boundaries for avoiding the electrojets, but we have checked that the data used give relatively consistent results across a range of observatory latitudes and for storms of various intensities.

[9] From the chosen observatories, and consistent with the standard calculation of Dst , we only use the horizontal-intensity H component. For observatories on low magnetic latitudes, H is the vector component most affected by the ring current. Storm time induced currents in the lithosphere and mantle contribute a substantial signal to the vertical vector component Z , and so it is almost never used for ring current studies. For each storm that we map, we visually inspect the H data from each candidate observatory for overall fidelity, checking for obvious problems. For the most part, the data are of very high quality, but in a few cases, we choose not to use parts of some of the available time series. A subset of the acceptable data are selected for each year from observatories having relatively good uniformity in site longitudes and a variety of site latitudes. For movie-maps for the years 1999–2006 (solar cycle 23), we use data from between 20 and 25 observatories

Table 1. Summary of Magnetic Observatories Providing Data for the Movie-Maps

Observatory	Code	Geographic		Magnetic		Supporting Institutes
		λ_G (°N)	ϕ_G (°E)	λ_B (°N)	ϕ_B (°E)	
Alma Ata	AAA	43.25	76.92	34.29	152.74	Institute of the Ionosphere, Kazakhstan
Alibag	ABG	18.64	72.87	10.19	146.16	Indian Institute of Geomagnetism
Apia	API	-13.81	188.22	-15.36	262.65	Samoa Meteorology Division and Institute of Geological and Nuclear Sciences, New Zealand
Beijing Ming Tombs	BMT	40.30	116.20	30.13	187.04	Chinese Academy of Sciences
Stennis	BSL	30.35	270.37	40.05	339.79	U.S. Geological Survey
Charters Towers	CTA	-20.09	146.26	-28.01	220.97	Geoscience Australia
Del Rio	DLR	29.49	259.08	38.30	327.31	U.S. Geological Survey
Zhaqing	GZH	23.09	113.34	12.88	184.84	China Earthquake Administration
Hartebeesthoek	HBK	-25.88	27.71	-27.13	94.40	National Research Foundation, South Africa
Hermanus	HER	-34.42	19.22	-33.98	84.02	National Research Foundation, South Africa
Honolulu	HON	21.32	202.00	21.64	269.74	U.S. Geological Survey
Kakioka	KAK	36.23	140.19	27.37	208.75	Japan Meteorological Agency
Kakadu	KDU	-12.69	132.47	-21.99	205.61	Geoscience Australia
Kanoya	KNY	31.42	130.88	21.89	200.75	Japan Meteorological Agency
Kourou	KOU	5.21	307.27	14.89	19.66	Institut de Physique du Globe de Paris, France
Lunping	LNP	25.00	121.17	14.99	192.14	Directorate General of Communication, Taiwan
Learmonth	LRM	-22.22	114.10	-32.42	186.46	Geoscience Australia
Lanzhou	LZH	36.09	103.84	25.86	176.08	China Earthquake Administration and Institut de Physique du Globe de Paris, France
M'Bour	MBO	14.38	343.03	20.11	57.47	Institut de Recherche pour le Développement, France
Midway	MID	28.21	182.62	25.02	249.50	U.S. Geological Survey
Memambetsu	MMB	43.91	144.19	35.35	211.26	Japan Meteorological Agency
Phu Thuy	PHU	21.03	105.96	10.78	177.85	Vietnamese Academy of Science and Institut de Physique du Globe de Paris, France
Pamatai	PPT	-17.57	210.43	-15.14	285.14	Institut de Physique du Globe de Paris, France
Qsaybeh	QSB	33.87	35.64	30.27	113.47	National Council for Scientific Research, Lebanon
San Fernando	SFS	36.46	353.79	40.09	73.18	Real Observatorio de la Armada, Spain
San Juan	SJG	18.11	293.85	28.31	6.08	U.S. Geological Survey
San Pablo–Toledo	SPT	39.55	355.65	42.78	75.98	Instituto Geografico Nacional, Spain
Tamanrasset	TAM	22.79	5.53	24.66	81.76	Centre de Recherche en Astronomie, Astrophysique et Geophysique, Algeria, and Institut de Physique du Globe de Paris, France
Antananarivo	TAN	-18.92	47.55	-23.67	115.78	University of Antananarivo, Madagascar
Teoloyucan	TEO	19.75	260.81	28.77	330.38	Ecole et Observatoire des Sciences de la Terre, France
Trelew	TRW	-43.25	294.68	-33.05	5.62	Universidad Nacional Autónoma de México Universidad Nacional de la Plata, Argentina, and Institut Royal Météorologique, Belgium
Tucson	TUC	32.17	249.27	39.88	316.11	U.S. Geological Survey
Vassouras	VSS	-22.40	316.35	-13.29	26.61	Observatorio Nacional, Brazil

for each storm. This number is comparable to the number of observatory time series used by *Clauer et al.* [2003] (for magnetic latitudes $< 43^\circ$), and it is considerably more observatories than the 6 used by *Søraas et al.* [2006].

3. Satellite Data

[10] We use solar wind density n , velocity V , and interplanetary magnetic field vector data expressed in geocentric solar magnetospheric (GSM) coordinates (magnetic dusk B_y , magnetic north B_z) collected by the Advanced Composition Explorer (ACE) [Stone *et al.*, 1999], GEOTAIL [Nishida, 1994], and WIND [Russell, 1995] spacecraft. With these data, we can calculate solar wind pressure P on the magnetosphere. Since 1997, ACE has orbited outside the magnetosphere and in front of the bow shock at the L1 Lagrange point, about 1.5 million km from the Earth and toward the Sun on the Sun-Earth line. Since the solar wind

advances outward from the Sun, ACE measures the interplanetary medium prior to its arrival at the Earth. This makes the ACE data extremely valuable for predicting the imminent occurrence of a magnetic storm some 20 or 30 min in advance. Unfortunately, the ACE data time series are rather frequently discontinuous. In particular, solar wind sensors often do not properly operate during periods of strong enhancement of solar wind, a problem caused by the penetration of MeV protons through the shielding of the solar wind sensors. For this reason, and when ever possible, we fill in gaps in the ACE data with data from the other satellites. Since 1992, GEOTAIL has orbited the Earth and Moon in a highly elliptical orbit which, as the satellite's name implies, is usually in the magnetotail; on the occasions when it is outside of the bow shock, GEOTAIL data are useful for monitoring ambient interplanetary conditions. Since 1994, WIND has orbited the Earth and the L1 and L2 Lagrange points. It is usually

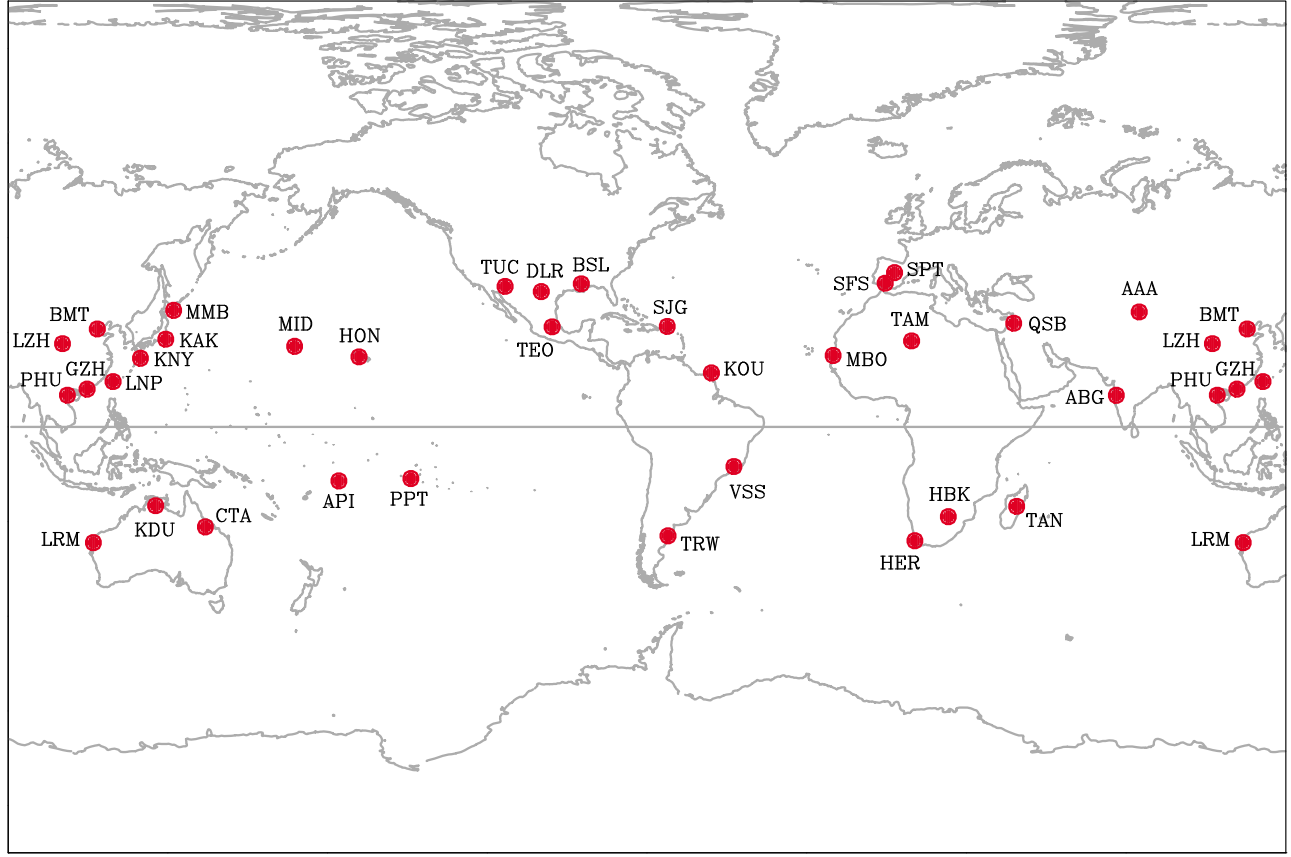


Figure 2. Map in geomagnetic coordinates showing the geographic distribution of magnetic observatories contributing data used in the movie-maps.

outside the bow shock, and so WIND data are also useful for monitoring ambient interplanetary conditions. For all three satellites, we use “contributed” (Level 3) 1 min average data obtained from NASA’s OmniWeb. These data have been ballistically propagated forward in time so that they correspond to proxy measurements made at the bow shock nose.

[11] We use magnetometer data from the geostationary GOES satellites [Singer *et al.*, 1996]. Depending on the year (1991–2006) data from the GOES 9, 10, 11 (225°E) and 8, 12 (285°E) are used. The data are reported in geographically fixed spacecraft coordinates, and we use only the north geographic component B_z . The GOES satellites, with their orbital radii of about $6.65 R_\oplus$, are usually within the magnetosphere and in the midst of the ring current. On occasion, however, during periods of highly enhanced solar wind pressure, the magnetopause is pushed in sufficiently far toward the Earth so that when the GOES satellites are on the dayside they can be within the magnetopause boundary layer. Most of the GOES data were obtained from NASA’s CDAWeb, but a large gap in those holdings (May 2005 to September 2005) was filled with data pro-

vided by P. T. M. Loto’Aniu (NOAA, personal communication, 2009).

4. Extraction of the Disturbance Field

[12] Observatory horizontal-intensity time series contain several superimposed signals in time t :

$$H(t) = C + SV + Sq + SC + Dist; \quad (1)$$

compare with Sugiura [1964, equation (1)]. C is permanent crustal magnetization; SV is the main field and its secular variation generated by the dynamo in the Earth’s core; Sq is solar quiet variation that has its primary source in ionospheric electric currents, but where magnetospheric and induced telluric currents contribute as well; and SC is any long-term, cyclical or secular variation associated with the solar cycle. The disturbance time series $Dist$ is dominated by magnetic storms and it is the focus of our mapping project here. In terms of mathematical adjectives, the $Dist$ field is transient, nonstationary magnetic variation that is very distinct from the steady C field, the long-term

decadal SV and SC fields, and the shorter-term, but stationary, harmonic Sq field.

[13] These qualitative differences facilitate a separation of the constituent parts of H and the isolation of the $Dist$ field; we use a time and frequency domain filtering method that is inspired by standard methods used to prepare observatory data for the calculation of Dst [Sugiura, 1964; Sugiura and Kamei, 1991]. In detail, our method is almost identical to that given by Love and Gannon [2009] and Gannon and Love [2010], modified slightly for application to shorter time series. We briefly summarize here. We work with 1 year units of observatory minute data. Magnetic signals that are much longer in time scale than magnetic storms, and longer in time scale than 1 year,

$$L(t) = C + SV + SC, \quad (2)$$

are well modeled over a finite time domain with a truncated Chebyshev polynomial. This polynomial is fitted to quiet-day data using a least squares algorithm, and it is subtracted from each horizontal intensity data, denoted with the subscript i , leaving an external-field combination of solar quiet and disturbance variation:

$$H_i - L(t_i) = E_i = Sq_i + Dist_i. \quad (3)$$

Next, large magnetic storms are identified in the E time series with a simple algorithm that searches for periods of unusual negative (or, even, positive) disturbance. These stormy periods are removed and, along with any data gaps, filled with interpolated values that mimic simple diurnal variation of Sq ; we call this time series Q because it closely approximates the Sq time series.

[14] The model solar quiet time series is constructed by cleaning Q in the frequency domain: we apply a Fourier transform

$$\mathcal{F}(Q_i) \rightarrow q_i; \quad (4)$$

see the power spectra given in Figure 3. We band-pass filter the Fourier coefficients corresponding to diurnal variation,

$$\mathcal{B} \cdot q_i = sq_i. \quad (5)$$

We do not filter for monthly and annual solar quiet harmonics, as Love and Gannon [2009, equations (11) and (12)] did, because those harmonics cannot be well resolved with the relatively short 1 year time periods considered here. Upon inverse Fourier transformation back into the time domain, we obtain the model solar quiet variation

$$\mathcal{F}^{-1}(sq_i) \rightarrow Sq_i. \quad (6)$$

When this is subtracted from the external field E , we are left with the sought-after disturbance field,

$$Dist_i = E_i - Sq_i. \quad (7)$$

[15] And, finally, each disturbance datum from each disturbance time series is weighted by $1/\cos \lambda_B$, where λ_B is the observatory site's magnetic latitude (Table 1). This transforms observatory-local horizontal disturbance data into the equivalent of disturbance data measured on the magnetic equator under the assumption of a uniform cylindrical-solenoidal-current source. For reasons outlined by Love and Gannon [2009], our method for removing Sq resolves certain small biases in the corresponding "standard" method defined by Sugiura [1964] and Sugiura and Kamei [1991]. Our method is also very different from that used, for example, by Clauer *et al.* [2003].

5. Plotting Conventions

[16] Example horizontal-intensity disturbance time series, $Dist$, from 24 observatories recording the Halloween storm of October 2003 are shown in Figure 4. To first order, the magnetograms from different observatory site longitudes are similar. Good correlation is seen over time scales of hours and longer, an observation that supports the general belief that data from just a few stations can be used to obtain an accurate estimate of average low-latitude magnetic disturbance (Dst). But close inspection of Figure 3 also shows important differences over short time scales. Note, for example, the first 1.5 hours of the storm. At some local times, disturbance is positive, while at other local times it is negative. Other differences in detail, which clearly have local time dependence, can be seen in the storm's two main phases.

[17] From these and other observations of the rich complexity of storm time magnetograms, it is evidently non-trivial to use a simple stack plot of magnetograms to relate local time differences in disturbance to processes occurring in a magnetospheric reference frame and over universal time. One way of obtaining a panoramic view of the data is to make contour plots of magnetic disturbance across a domain of local time and universal time [Zaitzev and Boström, 1971; Clauer and McPherron, 1974; Clauer *et al.*, 2003; Søraas *et al.*, 2006]. We will use such plots, but we also appreciate the utility of plotting data in a geometry that bears a resemblance to the physical system of interest, especially, if the plotting scheme permits detailed inspection of the data, their variation in time and their variance in space.

[18] Toward that end, we use a slightly unusual polar coordinate system to display storm time disturbance; see, for example, Figure 5, which represents a snapshot in time from one of our movie-maps (see caption for details). Each instantaneous disturbance value $Dist_i$ from each observatory is plotted radially (Figure 5f), where the zero value is on a circle centered at the origin. This permits unambiguous plotting of disturbance data that are positive (inside the zero-value circle) and negative (outside the circle). The azimuthal angle used for plotting each $Dist_i$ value is the local magnetic time for the observatory. The disturbance

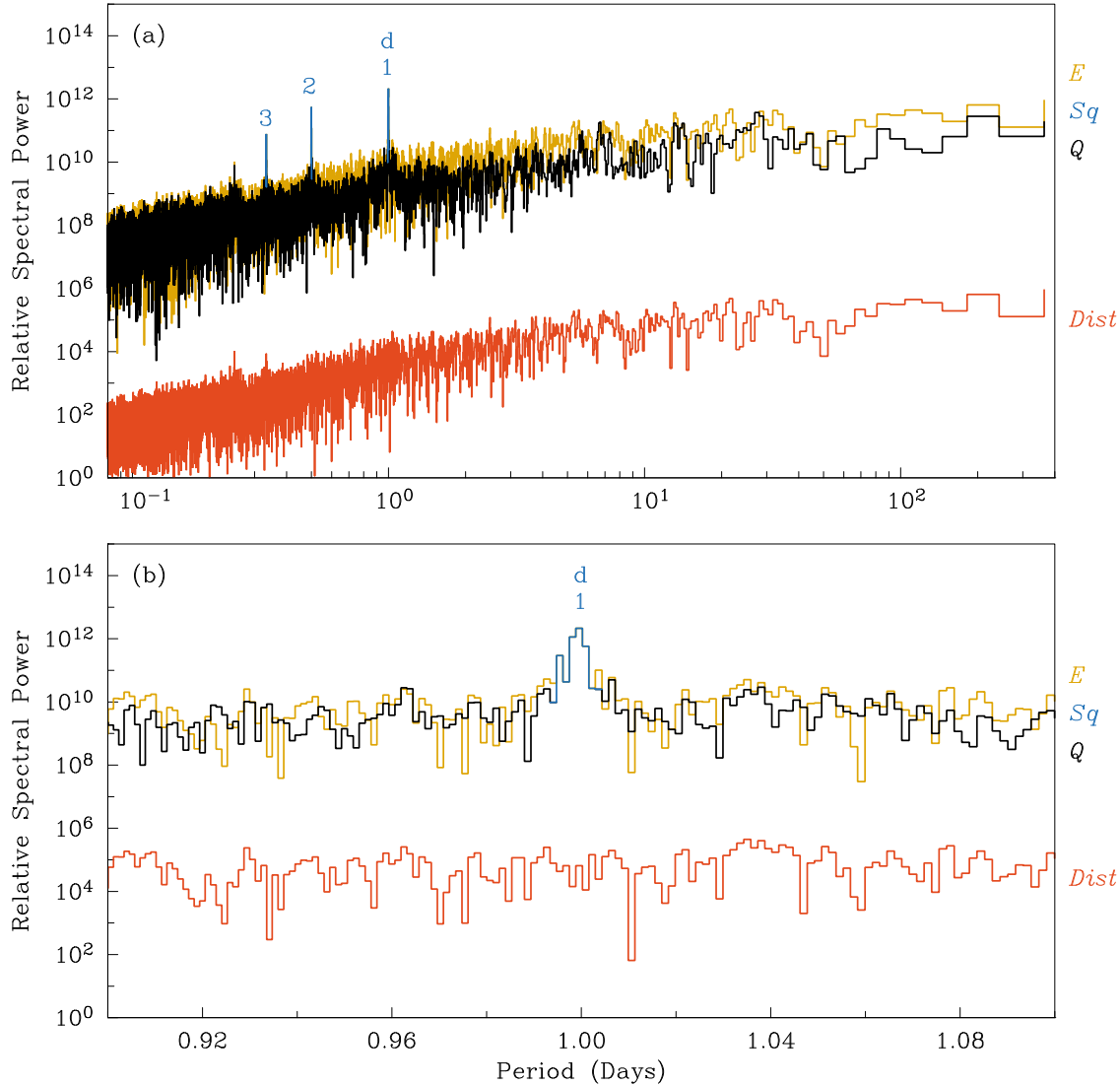


Figure 3. Relative power spectra for horizontal-intensity data from Alibag (ABG) for 2003. Shown are spectra for (a) periods of 0.08–400 days and (b) periods in the neighborhood of 1 day, in each case for the external-field E time series, the disturbance-interpolated time series Q , the solar quiet variation Sq , and the residual disturbance time series $Dist$. Labels show spectral peaks corresponding to diurnal (d) harmonics.

data for each universal time minute are fitted in local time with a truncated Fourier series

$$Dist(\theta_m) = Dst + \sum_{i=1}^3 a_i^c \cos\left(\frac{2\pi i \theta_m}{1440}\right) + \sum_{i=1}^3 a_i^s \sin\left(\frac{2\pi i \theta_m}{1440}\right), \quad (8)$$

where θ_m is local magnetic time measured in decimal minutes of day. The first term in the Fourier expansion is an azimuthally independent radial offset. This represents the local time (longitudinal) average of the disturbance curve, and it can be interpreted as an accurate estimate of Dst as

extracted from all of the observatory data. The model parameters (Dst, a_i^c, a_i^s) are obtained with a least squares algorithm, and the smooth curve $Dist(\theta_m)$ is plotted in polar coordinates. Our choice, here, of a decomposition in terms of Fourier terms is obviously motivated by a need for a complete basis set that is periodic in local time. Our choice for truncating the Fourier expansion, at degree 3, is the same as that of Clauer and McPherron [1974].

[19] In Figure 5, the Dst time series is plotted twice, once at the top (a) as a 7 day panoramic view of each storm's local time average disturbance and once (b) as a detailed 1 day close-up centered on the given instantaneous time.

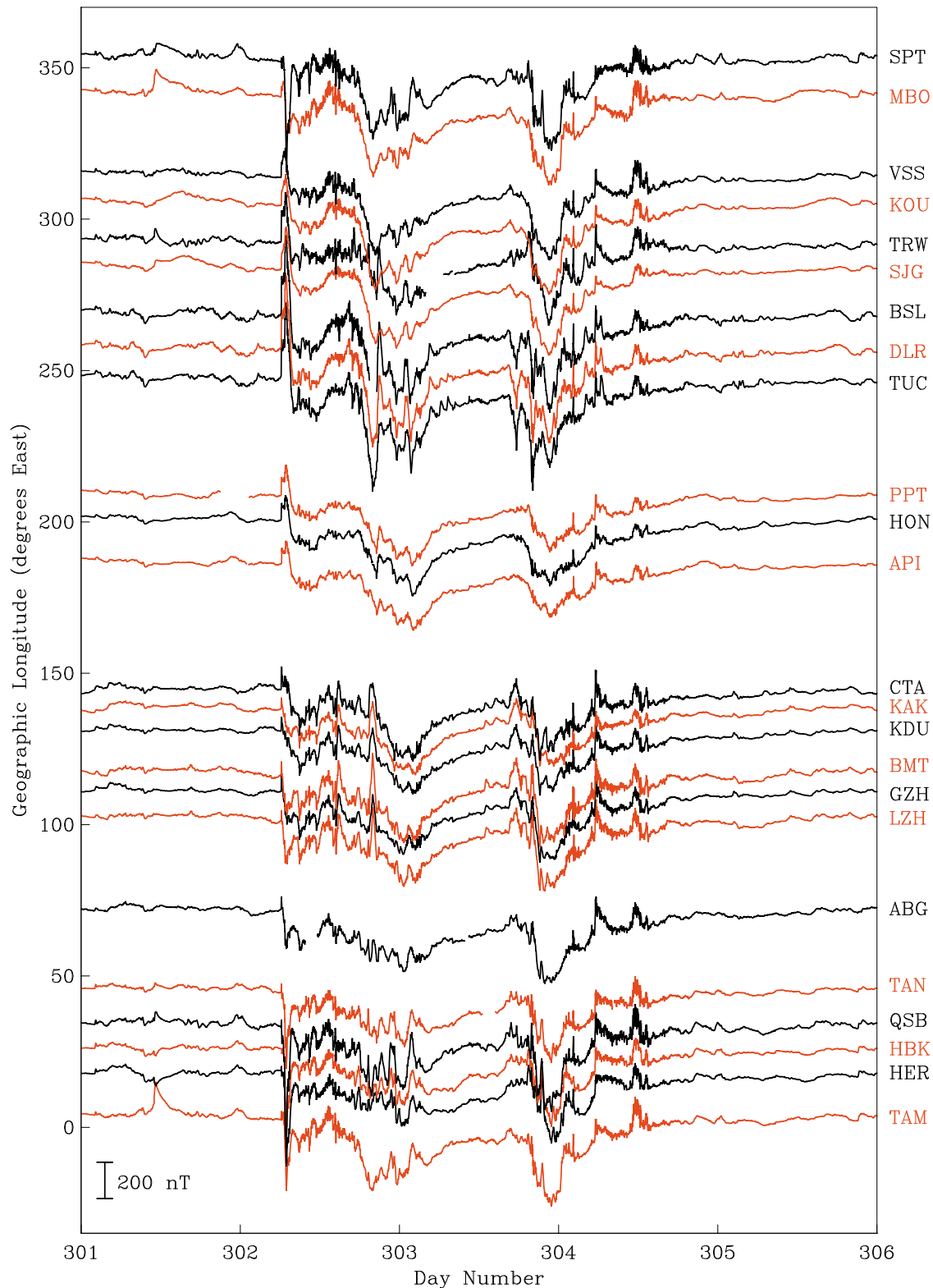


Figure 4. Stack plot of horizontal-intensity disturbance time series, $Dist$, from a longitudinal necklace of observatories recording the Halloween storm: 28 October to 1 November 2003.

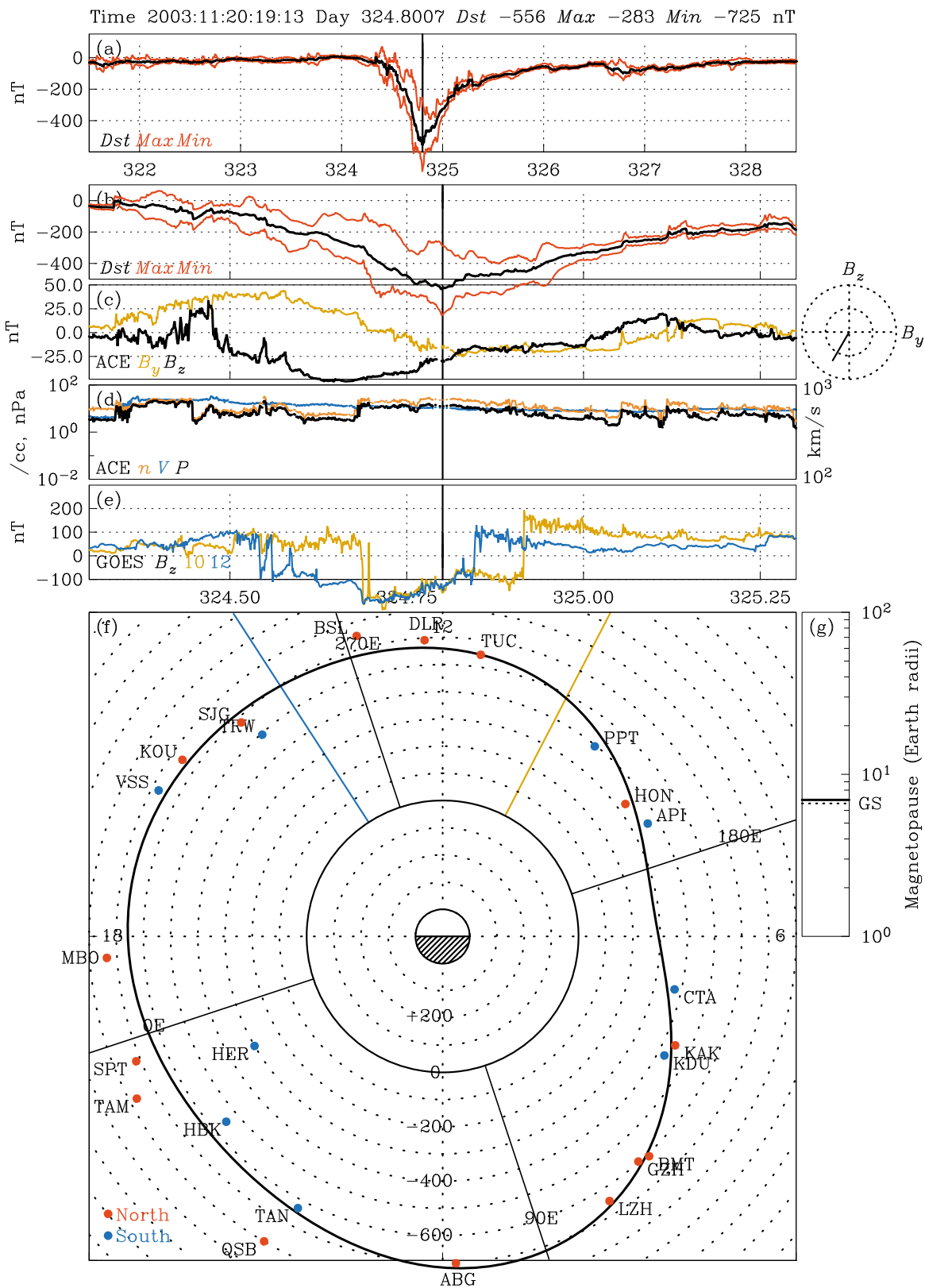


Figure 5

In both (a) and (b) we also plot the local time maximum and minimum value of $Dist(\theta_m)$. With respect to the ACE/GEOTAIL/WIND magnetic field data, in (c) the B_y and B_z components (dusk and north in GSM coordinates) are plotted as time series and, also, as an instantaneous value in polar coordinates which makes the clock angle, $\tan^{-1}(B_y/B_z)$, visually clear. In (d) we plot solar wind proton number density n , velocity V , and the calculated solar wind pressure P . In (e) we plot the GOES (east and west) north B_z magnetic component time series. And, finally, in (g) we plot the instantaneous subsolar magnetopause distance as determined by a simple balance between solar wind pressure and the magnetic pressure of the Earth's dipole and its image outside the magnetopause [e.g., *Chapman and Ferraro, 1930; Prölss, 2004*]. As already mentioned, all solar wind parameters used here have been propagated forward in time so that their time stamps correspond very nearly to those of the magnetic observatory data.

[20] Movie-maps are made by first generating a sequence of still plots of the format shown in Figure 5, one for each minute over a duration of time that encompasses most or all of the evolution in time of a chosen period of magnetic disturbance. There are, of course, many ways to generate still plots; we use a Fortran code that generates disturbance time series and a large number of format and command files. We then apply a simple plotting program that gives postscript output. These are converted into pdf files, useful for detailed inspection, and gif images that are concatenated into a movie. We use Apple Inc.'s QuickTime Pro (a trademark of Apple Inc., registered in the U.S. and other countries) for constructing mov-format movies which can be displayed with controls using normal QuickTime software (www.apple.com).

6. Results

[21] In Table 2 we list 29 movie-maps, each of which are freely available at the USGS Geomagnetism Program Web site (<http://geomag.usgs.gov>). The collection of movie-maps encompasses most of the large storms that occurred during solar cycle 23, including the great storm of November 2003 which had a maximum $-Dst_M$ of 561 nT. Also included in the collection is a movie-map of an

unusual period of magnetic quiescence. In one important case, for the storm of 2000:04:06 (YEAR:MN:DY), generating a movie-map was problematic because critical observatories were either temporarily not in operation or the data are defective in some way, so no movie-map for this storm is reported here. Still, this is more the exception than the rule, since the observatories typically deliver data with high fidelity and good continuity. Occasional operational problems were more of an issue for the interplanetary monitoring satellites. The most unfortunate example of this is the lack of high-resolution (1 min) solar wind data from ACE and WIND recording the Halloween storm of October 2003; GEOTAIL provided a small amount of data, but not during the critical early phases of this important storm. For some other storms, we use GEOTAIL or WIND in place of missing ACE data, for example, the Bastille Day storm of July 2000.

[22] Other than the unusual quiet time recorded in the movie-map (1999:05:11), all of the other movie-maps record one or more storms, each having the requisite main and recovery phases. Many of the movie-maps also record sudden impulses and initial phases as well. Watching the movie-maps makes it clear that each large magnetic storm has its own personality. Some storms have a rapid and complicated time dependence in terms of Dst and low-latitude magnetic disturbance asymmetry. Other storms are relatively slow and simple. Although we have chosen, in this analysis, to use data from observatories that should record the signal of the magnetospheric equatorial ring current, it is important to recognize that the $Dist$ time series is a superposition of magnetic signals, including those originating from currents in the magnetopause, the magnetotail, and the ionosphere. In the continuum that is the reality of the Earth's space environment, all of these currents are, to some degree, coupled together. It is not, therefore, surprising that our movie-maps show magnetic disturbance having a wide variety of temporal and spatial complexity.

[23] Still, the movie-maps show a reasonably coherent storm time signal. This is true, despite the fact that each observatory time series has been separately processed by staff from each supporting institution. Each time series has had a different time-dependent quiet time baseline removed, and each has been weighted according to the

Figure 5. Format used for movie-maps (example still from the great November 2003 storm). Time is indicated at the top in YR:MN:DY:HR:MN format and in terms of decimal day of year. Dst and maximum and minimum $Dist$ as determined by equation (8). The Dst and $Dist$ time series (a) for 7 days of time and (b) for 1 day of time centered on the time stamp given at the top. (c) ACE/GEOTAIL/WIND interplanetary magnetic field, B_y and B_z . (d) ACE/GEOTAIL/WIND solar wind ion density n , velocity V , and pressure P . (e) GOES east and west magnetic field, B_z . (f) Polar coordinate plot showing horizontal-field disturbance $Dist(\theta_m)$ (equation (8)). We also plot the individual instantaneous disturbance values, $Dist_i$, according to the observatory's local magnetic time, and each value is labeled with the standard IAGA three-letter code. A red (blue) dot denotes an observatory in the magnetic northern (southern) hemisphere. Geographic longitudes (0°E, 90°E, 180°E, and 270°E) are shown. For the years 1999–2006 and for low latitudes, a geographic longitude can be reasonably accurately translated into geomagnetic longitudes by subtracting 72.07°. The GOES east and west longitudes are indicated. (g) Estimated magnetopause distance; geostationary distance is labeled.

Table 2. Summary of Movie-Maps^a

Year	Month	Day	$-Dst_M$	Number of Observatories	Solar Wind Data	Comments
1999	4	17	121	21	ACE	Simple, almost linear piecewise evolution of Dst
1999	5	11	—	20	ACE	The day the solar wind disappeared
1999	9	22	198	20	ACE	
1999	10	22	236	20	ACE	
2000	7	16	397	24	ACE and GEOTAIL	Isolated initial phase, Bastille Day storm
2000	8	12	244	23	ACE	
2000	9	17	244	24	ACE	
2000	10	5	192	24	ACE	
2000	11	6	175	23	ACE	
2001	3	20	166	22	ACE	Storm, followed by activity, no KOU, VSS data
2001	3	31	398	24	ACE	Isolated initial phase, large but brief sudden impulses, then large storm
2001	4	11	310	23	ACE	Isolated initial phases, storm with very asymmetric early main phase
2001	10	3	191	24	ACE	
2001	10	21	212	24	ACE	
2001	10	28	139	23	ACE	Two medium size storms
2001	11	6	298	23		Large sudden impulse, large storm, but no solar wind data
2001	11	24	233	24	GEOTAIL	Interesting large asymmetries, no ABG data
2002	4	20	154	22	ACE	
2002	9	8	180	23	ACE	
2002	10	1	173	21	ACE	No ABG data
2003	10	30	429	24		Spectacular Halloween storm, two steps, no 1 min solar wind data
2003	11	20	561	24	ACE	Largest storm in movie-map collection
2004	7	27	222	24	ACE	Long duration of activity, or three storms
2004	11	8	348	23	ACE	Long complex, two-step storm with all phases represented
2005	5	15	283	25	ACE	Distinctive initial phase, no API data
2005	5	30	125	23	ACE	No API, MBO data
2005	8	24	193	23	GEOTAIL	Very asymmetric, no API data
2005	9	11	129	24	WIND	No solar wind data during storm maximum
2006	12	15	172	25	ACE	

^a $-Dst_M$, maximum storm intensity. Largest storms are highlighted in bold font.

observatory's magnetic latitude. The fact that observatories from northern and southern hemispheres often show similar storm time disturbance variation, tells us that the data we are using are of high quality, that we are treating the data more or less correctly, and that interpretations that we and others might make in terms of large-scale magnetospheric current systems are probably reasonable. Occasionally, however, this coherence breaks down, as it does, to some degree, during some brief moments of very rapid field change, when the data sometimes show substantial scatter about the curve given by equation (8). This might be evidence for the existence of substantial, but transient, superposition of magnetic fields from different source regions. And when this happens, it is, of course, of interest.

[24] We give, now, a summary of some straightforward observations we have taken from the movie-maps; beginning with a discussion of the Halloween storm, followed by a general discussion of different storm phases from other storms together with some comparisons with the Halloween storm, and closing with a discussion of a period of magnetic quiescence. For this discussion we will use a simplified version of the format given in Figure 5; more detailed inspection requires viewing of the movie-maps.

6.1. Halloween Storm 2003:10:30

[25] The Halloween storm of October 2003 [e.g., Balch *et al.*, 2004; Gopalswamy *et al.*, 2005] was well recorded by

magnetic observatories, but the solar wind was not well recorded by any of the monitoring satellites considered here. The ACE solar wind monitor was almost overwhelmed, but Skoug *et al.* [2004] have managed to process the affected data (maximum $V > 2240$ km/s), but their time series has half-hour resolution, very coarse compared to the minute-mean observatory data considered here. Still, this storm was of unusual dimension and complexity, and it is, therefore, worthy of special examination.

[26] The storm begins with a sudden impulse, Figure 6 (a, DY:HR:MN, 29:06:13), which, in the first few minutes of the storm is marked a positive Dst of 31 nT. At this point, low-latitude disturbance is asymmetric; positive disturbance of about 150 nT is seen on the nightside, but very little disturbance, positive or negative, is seen on the dayside. Over the next hour or so (b), and as the storm enters its main phase, the asymmetry grows; at 29:06:57 we estimate $-Dst = 79$ nT and a local time range, $\text{Max Dist} - \text{Min Dist}$, of an enormous 867 nT. At this time there is significant scatter in the individual observatory disturbance fields at about 09:00 local time, and GOES 10 and 12 appear to indicate some degree of nightside dipolarization. At the end of this dynamic early phase (c, 29:07:39), $-Dst = 126$ and low-latitude disturbance becomes more symmetrical. This is followed by a complex period lasting about 11 hours when there is prominent dayside ultralow-

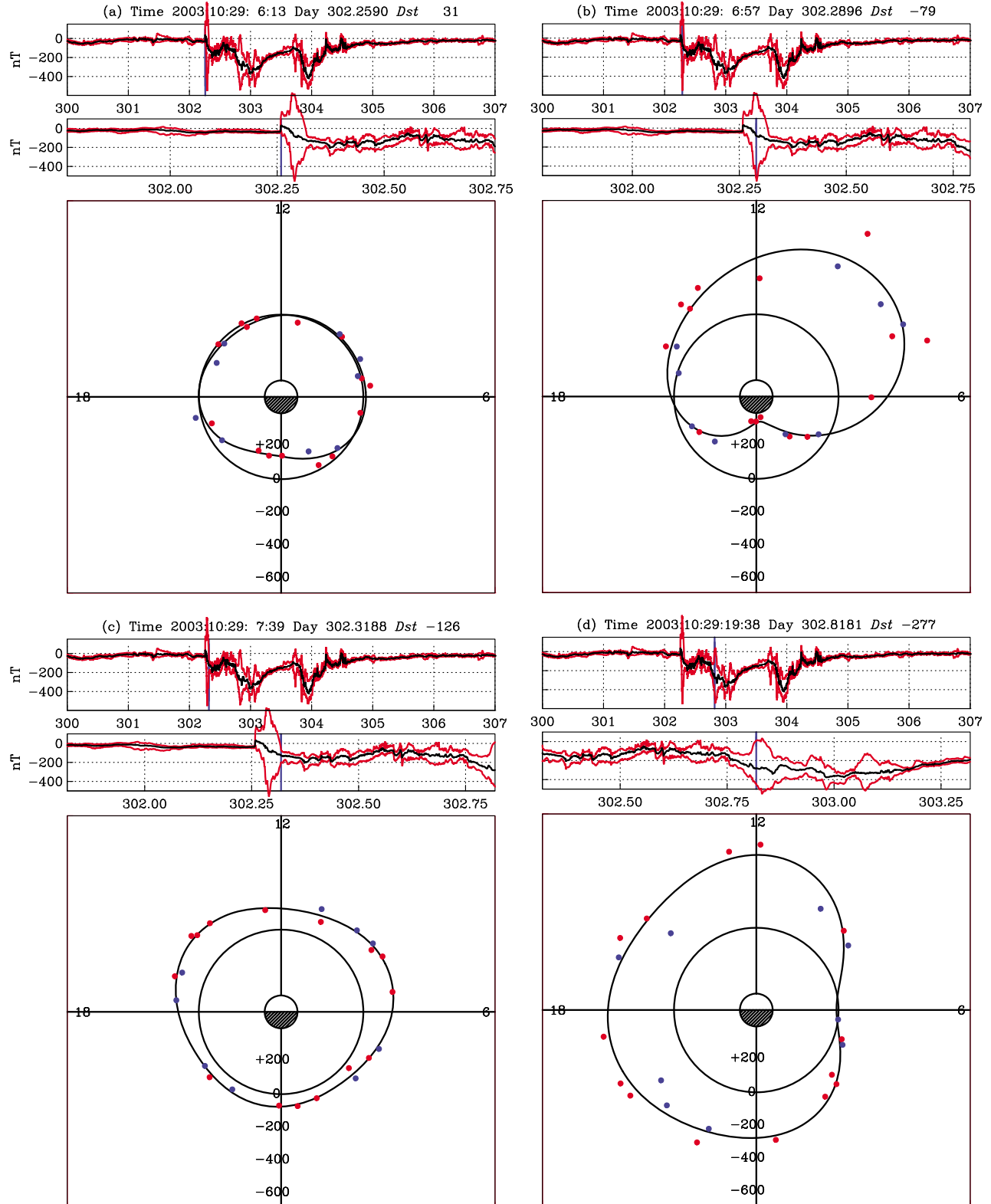


Figure 6. Simplified stills from the movie-map 2003:10:30 recording the Halloween storm. This storm is of great complexity, and many of the features seen in these stills and in the movie-map are seen in other storms as well.

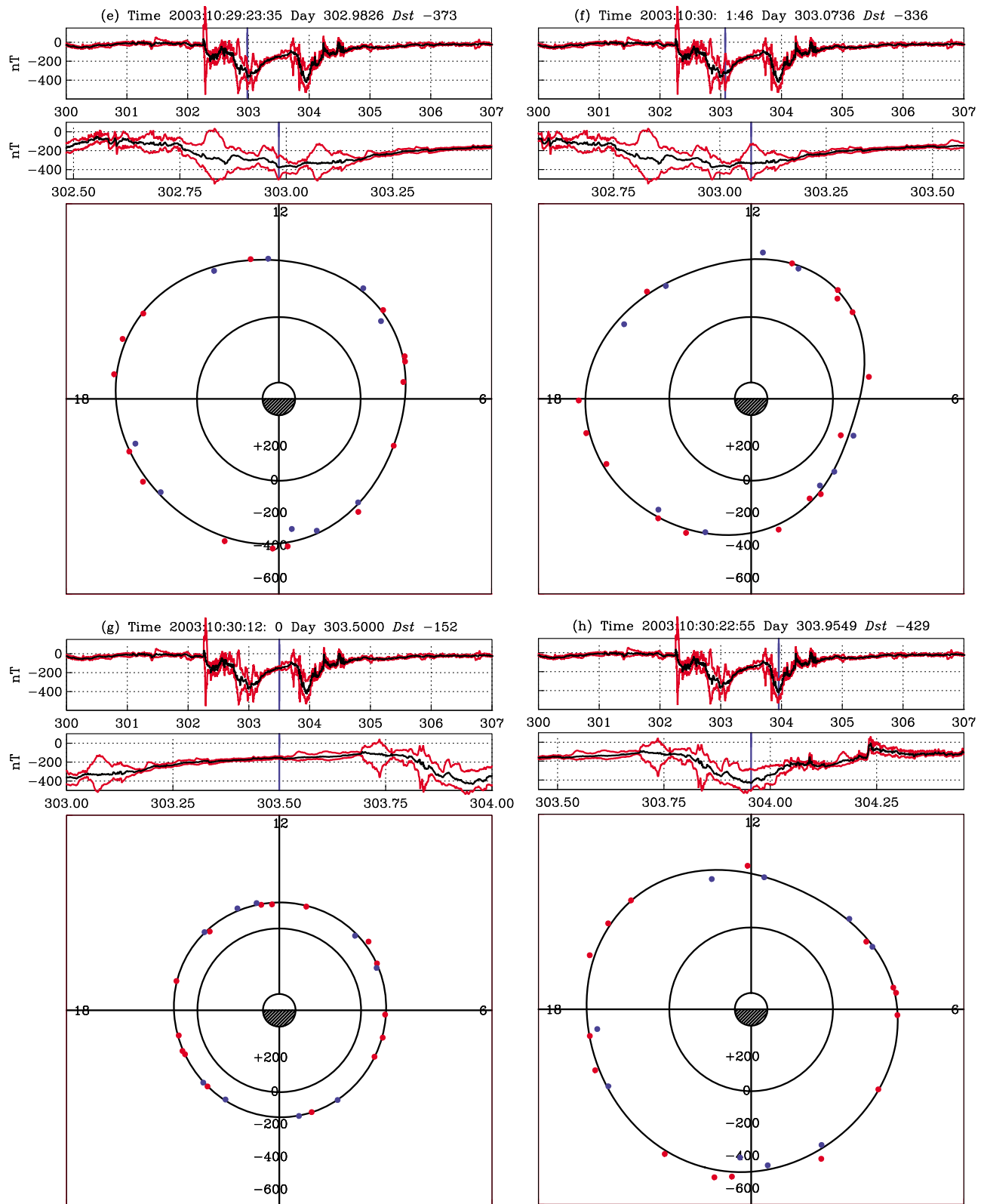


Figure 6. (continued)

frequency (ULF) variation with periods of a few minutes [e.g., *Panasyuk et al.*, 2004] (see movie-map).

[27] The storm enters (d, 29:19:38) the first of two main phase “steps” (in the vocabulary of *Kamide et al.* [1998a]), when disturbance shows substantial local time asymmetry; there is an almost complete collapse at dawn of magnetic disturbance as measured at observatories across a wide range of latitudes: China (BMT, GZH, LZH), Japan (KAK), and Australia (CTA, KDU). A brief duration of solar wind data from the GEOTAIL satellite is available at this time; the pressure is not unusually high, but the interplanetary magnetic field is essentially directed southward, with an intensity of about 25 nT (see movie-map), a situation which is well known to promote magnetospheric convection. A first-step maximum follows (e, 29:23:35), $-Dst_M = 373$ nT. After a subsequent period of asymmetry (f), storm partial recovery commences (g) with typically more symmetrical disturbance. The storm’s second step commences with alternating periods of symmetry and asymmetry (again, see movie-map). The storm attains its overall maximum (h, 30:22:55) with $-Dst_M = 429$ nT. Prominent ULF variation occurs during the second-step recovery phase [*Potapov et al.*, 2006].

6.2. Initial Phases

[28] The Halloween storm does not have a distinctive initial phase, such as those shown in Figure 7 for other storms. In Figure 7a the initial phase is essentially an isolated event, maximum $Dst = 84$ nT, although some 2 days later, after a period of magnetic quiescence, it is followed by the Bastille Day storm (2000:07:16). Consistent with the theory of *Chapman and Ferraro* [1930], the movie-map for this storm makes it clear that the onset of the isolated initial phase is caused by an enhancement of solar wind pressure. This pushes the magnetopause in toward the Earth and intensifies the eastward electric currents of the magnetopause. By Ampère’s law, the magnetopause currents generate a northward magnetic disturbance, and since the dimension of the magnetopause is much larger than the diameter of the Earth, positive magnetic disturbance is seen more or less uniformly at all local times; the curve fitted to the disturbance data is relatively symmetrical. Over the course of the next 5–7 hours, however, the disturbance of this initial phase becomes more asymmetrical, possibly in response to mild magnetospheric convection commencing with intermittent B_z south and connection of the interplanetary magnetic field onto the geomagnetic field.

[29] The main phase of the great storm of March 2001 was preceded by a large sudden impulse (Figure 7b, 31:01:00), maximum $Dst = 146$ nT, corresponding to the arrival of a sharp pressure pulse of about 100 nPa. *Russell et al.* [1992] estimate that an increase of $1 \text{ (nPa)}^{1/2}$ in the square root of solar wind pressure on the magnetopause produces a positive perturbation in Dst of 16.5 nT, and this matches well with the data for this sudden impulse. Note that the impulse is also prominently seen in the GOES data. The positive magnetic disturbance seen at all

local times in Figure 7b is not especially consistent with statements offered by *Skoug et al.* [2003, section 2.3]. The initial phases seen for the November 2004 storm are noteworthy for their tidy superposition, one arriving at about 07:03:05 and one subsequently arriving at 07:11:00, each associated with an increase in solar wind pressure (see movie-map). These initial phases eventually diminish, and, then, hours later, with the arrival of yet another increase in solar wind pressure, a new and substantial initial phase is supported (Figure 7c, 07:19:24). The May 2005 storm commences with a very prominent initial phase (Figure 7d, 15:02:53), one that persists at a more or less constant level for about 3.5 hours; as expected, it is correlated with an increase in solar wind pressure. In our opinion, there is very little that is controversial about these observations concerning storm initial phases.

6.3. Early Positive Asymmetry

[30] In Figure 8 we show four example maps of early storm time asymmetry in low-latitude disturbance. In (a), after a sudden impulse and before the storm’s main phase, positive disturbance is seen on the dayside, but, otherwise, disturbance is nearly zero; in (b), after a sudden impulse and before main phase, positive on the dawnside; in (c), after an initial phase and before main phase, positive on the nightside; in (d), in the middle of an initial phase, positive on the nightside. Although a variety of early storm asymmetry is certainly possible, on the basis of these simple observations, we can safely say that the early positive asymmetries seen in the Halloween storm (Figure 6a) and a similar asymmetry reported by *Clauer et al.* [2001] for the September 1998 storm, are not particularly unusual.

[31] As for an explanation for the early positive asymmetries shown in Figure 8, drawing general conclusions about disturbance asymmetry and interplanetary magnetic field orientation would require the examination of far more than just four specific moments in time from four independent storms. And we see no obvious correlation. Still, it is worth noting that for each case shown in Figure 8, solar wind pressure is enhanced to about 10 nPa, about an order of magnitude above normal quiet levels. When the movie-maps are viewed, it becomes clear that (a, b, c) are just instantaneous snapshots taken from continuous magnetic field evolution progressing from a symmetric initial phase, produced by enhanced solar wind pressure, toward a typically asymmetrical main phase, with a ring current that is possibly energized through particle injection in a limited range of local times. When described in these terms, it is not surprising that the first moments of some, and probably most, magnetic storms can exhibit occasional positive asymmetry.

6.4. Positive-Negative Asymmetry

[32] We next examine some instances of storm time asymmetry having a mixture of positive and negative disturbance across a range of local time, Figure 9. In (a) positive (negative) on the night (day) side, interplanetary

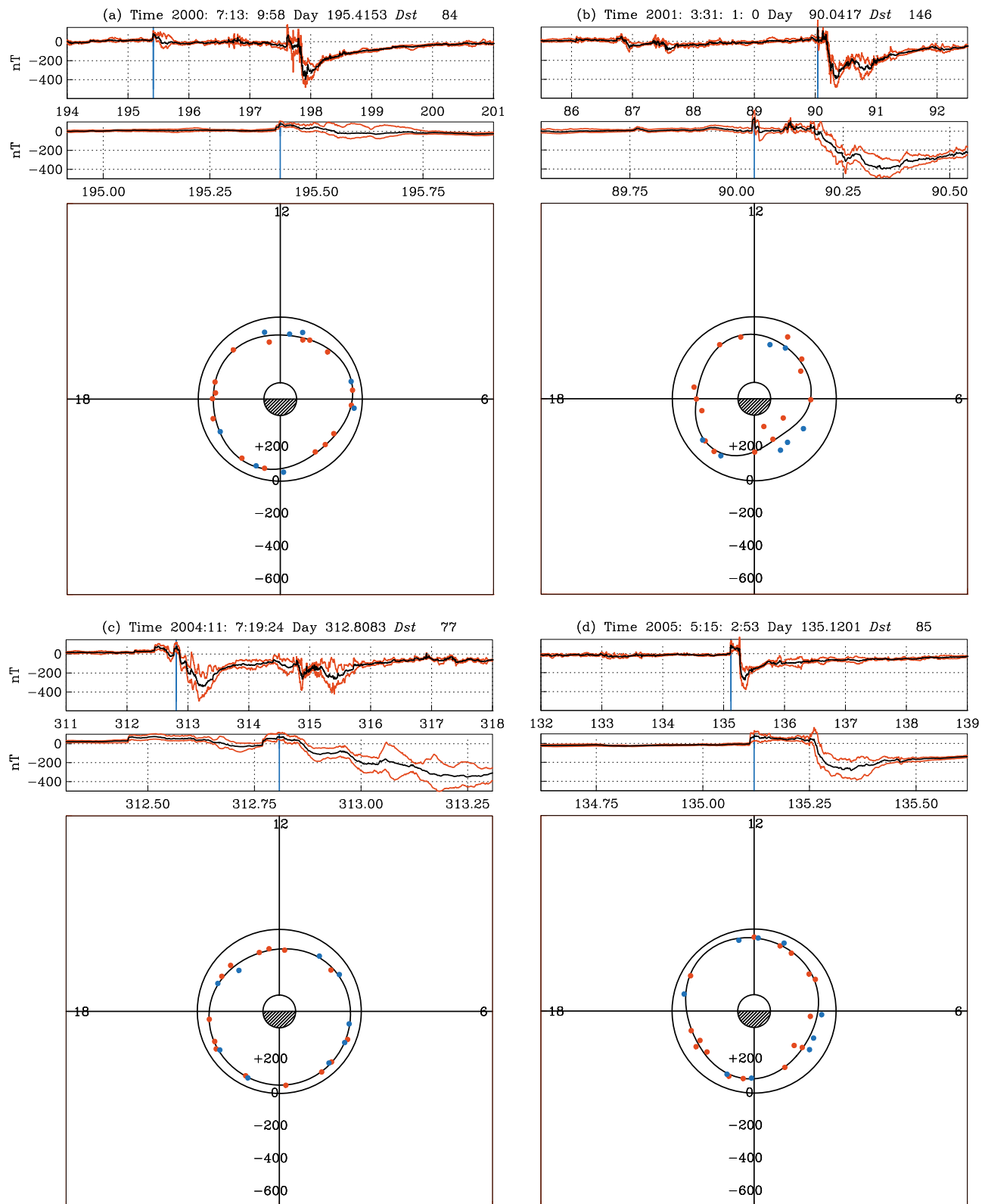


Figure 7. Stills from four different storms having a distinctive initial phase.

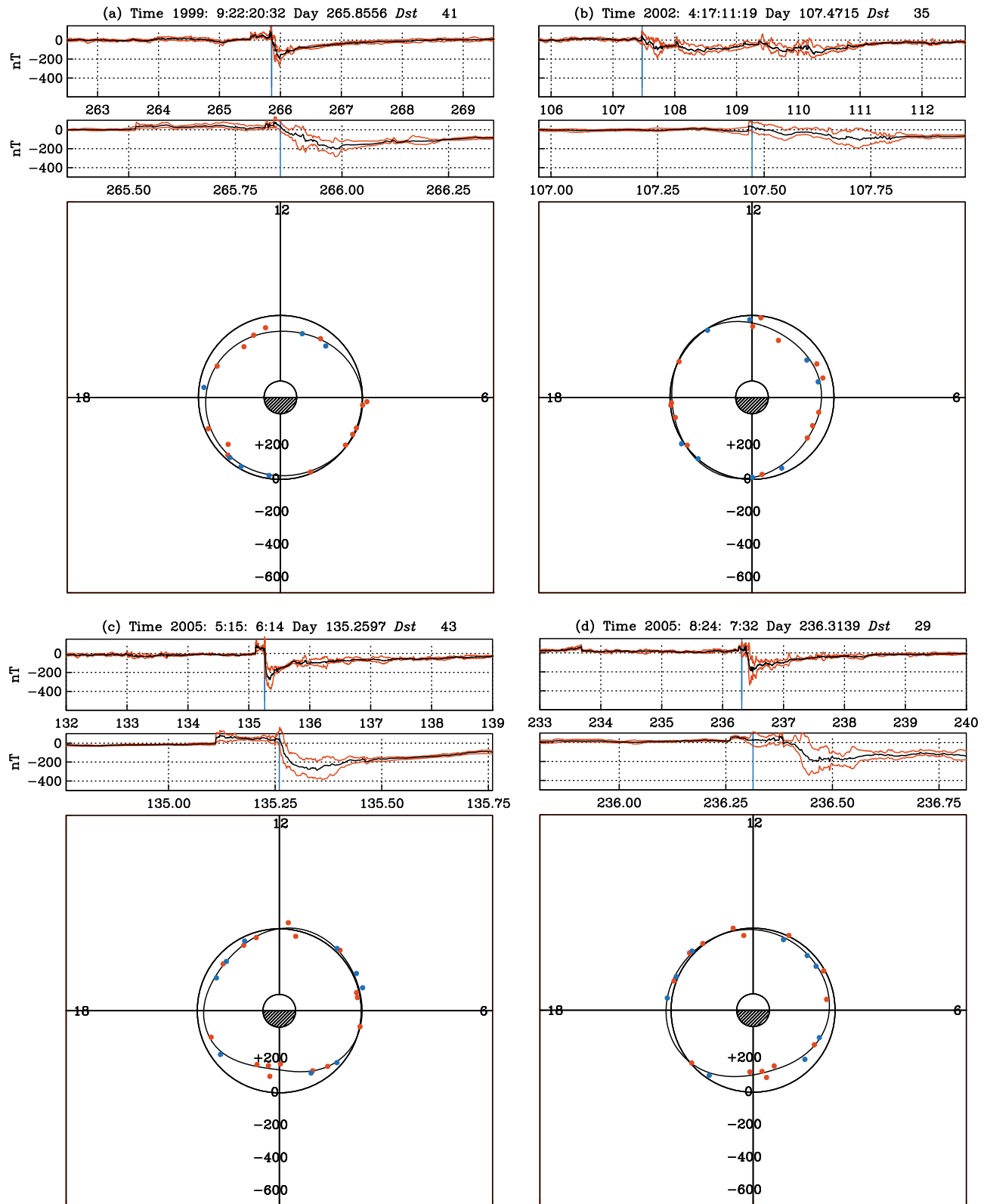


Figure 8. Stills from four different storms showing early positive asymmetry.

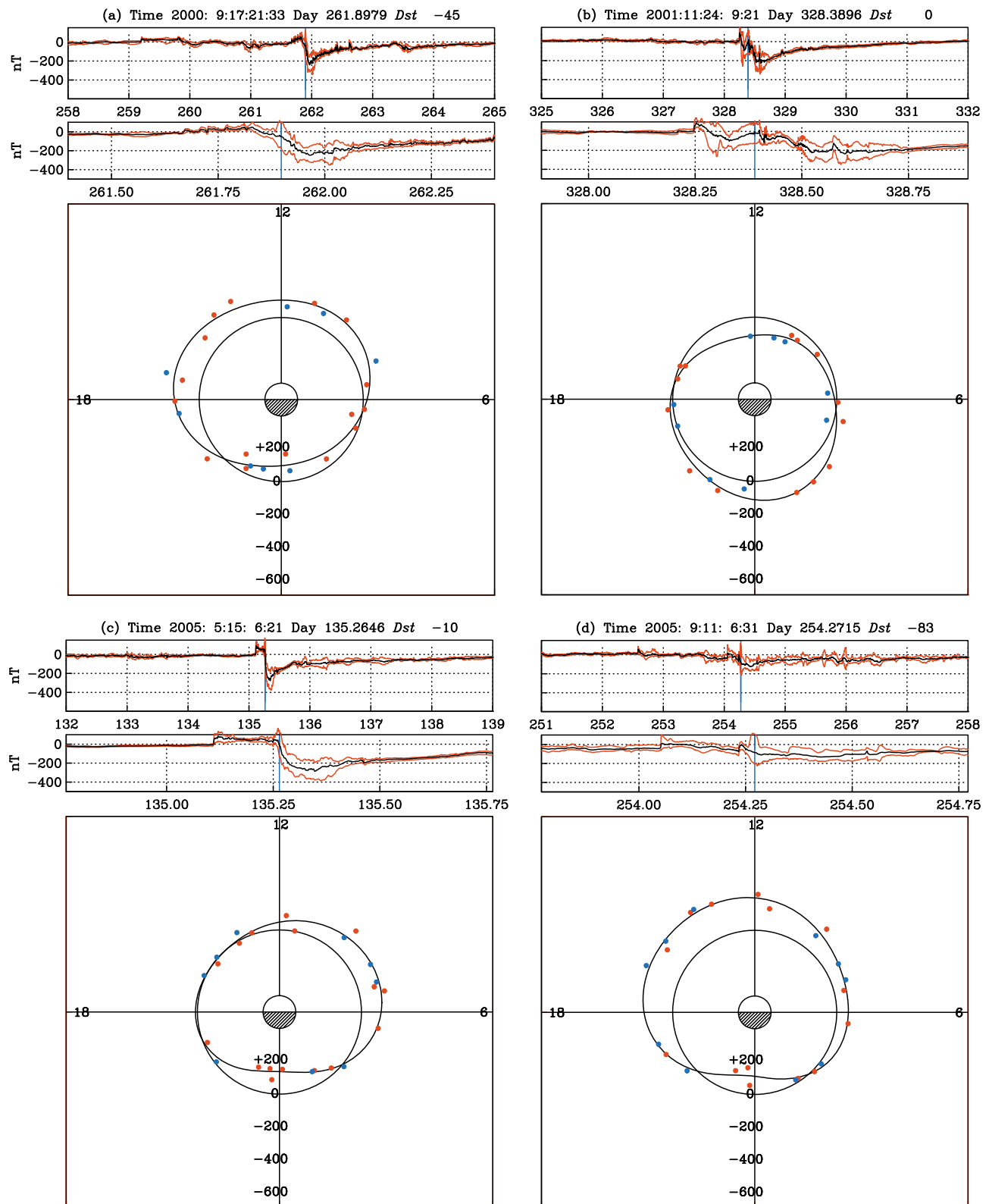


Figure 9. Stills from four different storms showing positive-negative asymmetry.

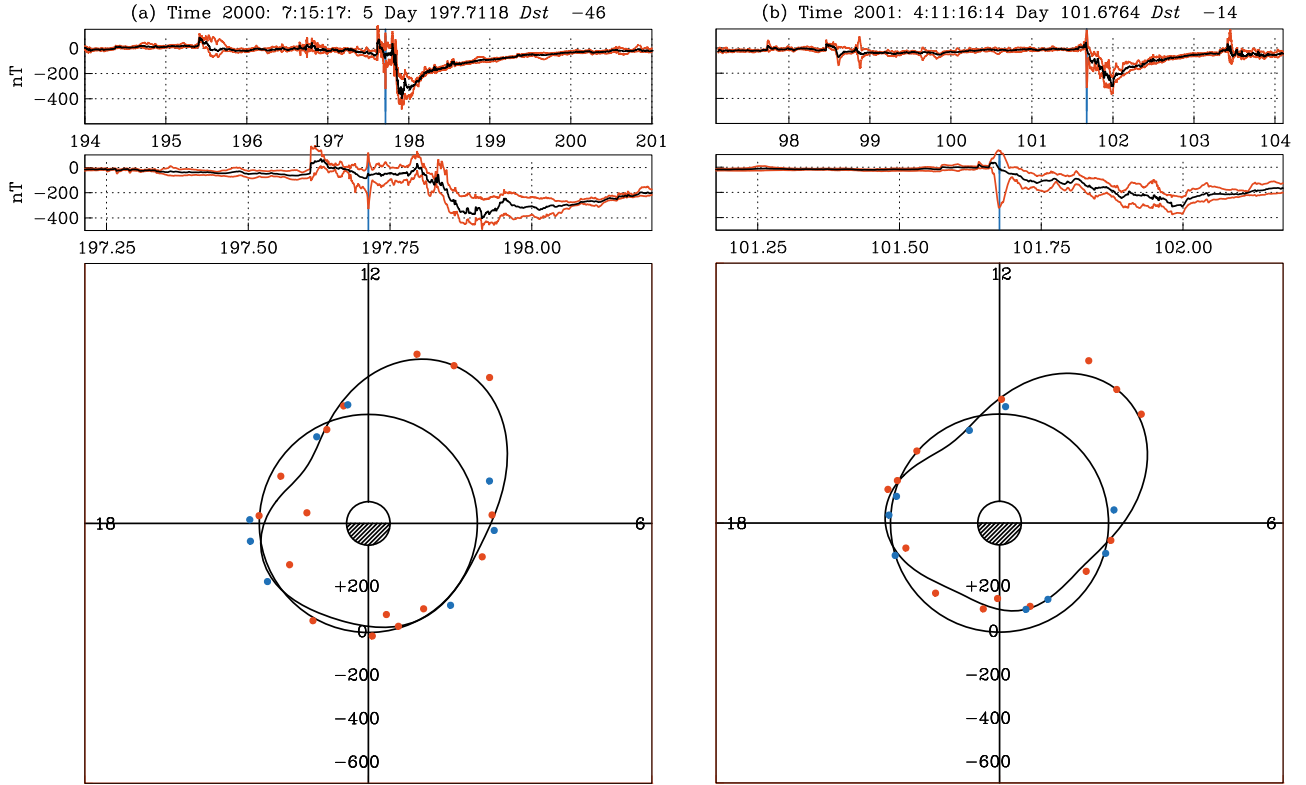


Figure 10. Stills from two different storms showing extreme negative asymmetry.

$B_z < 0$ (see movie-map); in (b) positive (negative) on the day (night) side, interplanetary $B_z > 0$; in (c) positive (negative) on the night (day) side, interplanetary $B_z < 0$; note that this instance is a subsequent snapshot of the storm shown in Figure 8c; in Figure 9d positive (negative) on the day (night) side, no reliable solar wind data. Here again, with only a limited number of examples, we do not feel we can draw general conclusions about disturbance asymmetry and the orientation of the interplanetary magnetic field. We note, however, that solar wind pressure in (a, b, c) is enhanced, especially for (b, 2001:11:24) when it approaches 100 nPa.

[33] We believe that Figures 8 and 9 are showing a superposition of disturbance sustained by magnetopause currents, supported by solar wind pressure, and partial ring currents (and, even, field-aligned currents) [Siscoe, 2006]. The latter can be realized at just about any local time, especially during highly dynamic storm evolution, but which might be rather often centered on the dayside during periods of enhanced solar wind pressure and $B_z < 0$, but, again, we are cautious about conclusions that

over reach. If this is true, then it might also explain the extreme asymmetry seen during the early main phase of the Halloween storm (Figure 6b). Shi *et al.* [2005] suggest that when interplanetary $B_z < 0$ ($B_z > 0$) solar wind pressure enhances (has little effect) on low-latitude magnetic disturbance. In light of their work, the storm (2001:11:24), with its extremely variable asymmetry under conditions of high solar wind pressure, might be a good candidate for a similar detailed study.

6.5. Extreme Negative Asymmetry

[34] In Figure 10 we show two examples of asymmetric disturbance that is extremely negative at about 09:00 local time. In Figure 10a during a rough initial phase of the Bastille Day storm, solar wind pressure has abruptly increased and interplanetary B_z has turned north (see movie-map). In Figure 10b the situation is seemingly very different, during early main phase, with solar wind pressure enhanced, but with $B_z < 0$. That these two independent instances of disturbance are visually so similar is rather surprising. The extreme negative asymmetry seen during

Figure 11. For three different storms. (a, d, g) The Dst and maximum and minimum Dst time series for 7 days of time. (b, e, h) Contour plots of horizontal-field disturbance $Dist$ over the local time and universal time domain, contour interval 100 nT. (c, f, i) Contour plots of the asymmetric part of the disturbance field $Asym(\theta_m) = Dist(\theta_m) - Dst$, contour interval 50 nT. Note the prominent dawn–dusk asymmetry in main phase disturbance.

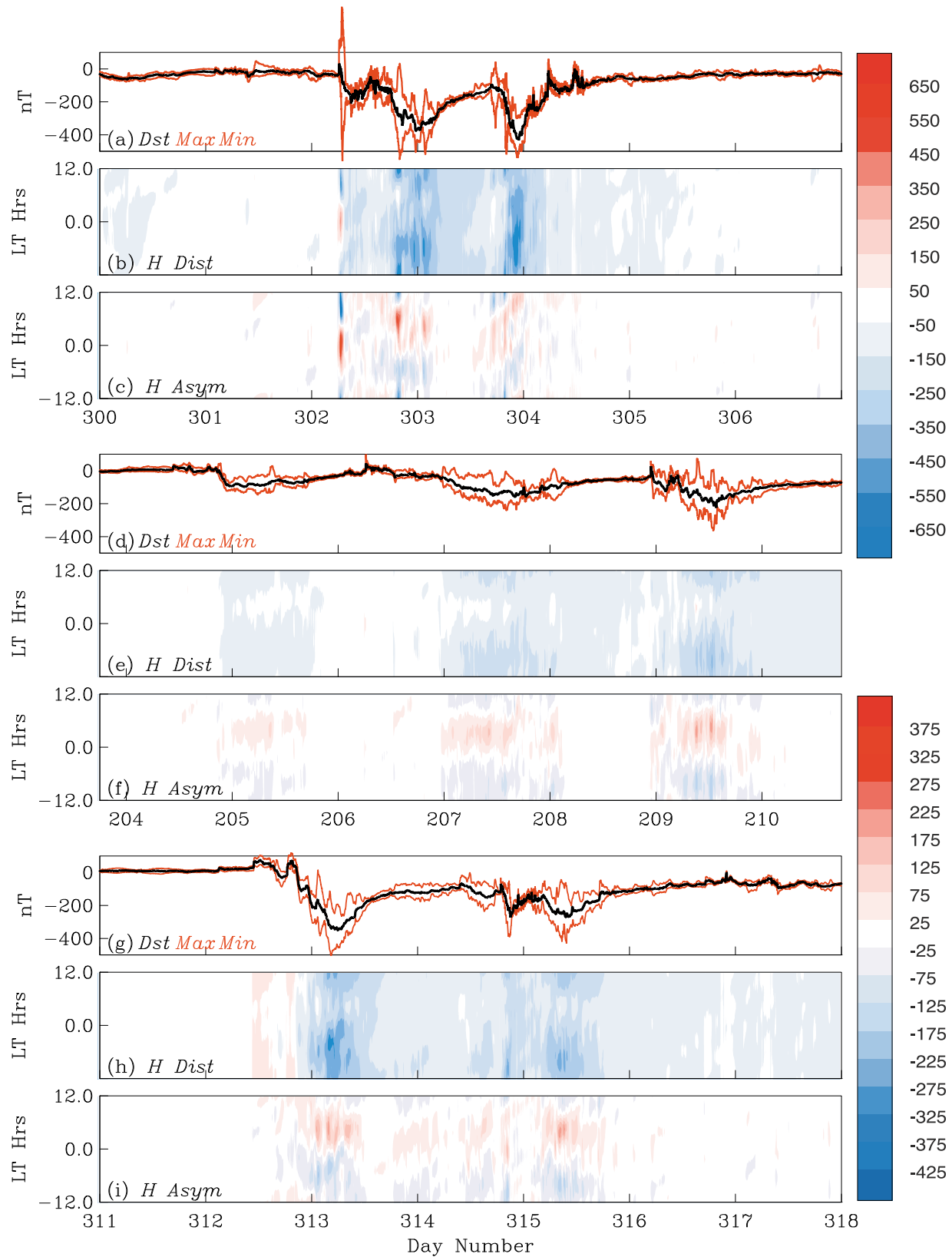


Figure 11

the early main phase development of the Halloween storm, Figure 6b, also at about 09:00 local time, might have some physical similarity to the disturbance shown in Figure 10b.

6.6. Main Phase Dawn-Dusk Asymmetry

[35] One of the clearest patterns seen in observatory storm time disturbance data is transient diurnal variation [Sabine, 1856; Moos, 1910a, 1910b], with greatest (least) negative storm disturbance seen in individual observatory time series at dusk (dawn) local time [Chapman and Bartels, 1962, chapters 6.8 and 9.3; Cummings, 1966]. This pattern is distinct from stationary diurnal solar quiet variation, but to resolve the dawn-dusk asymmetry in observatory data, it is important that the Sq signal be carefully removed before proceeding with an analysis of the Dst field. A Dst -scalable map of dawn-dusk asymmetry, based on 50 years of observatory disturbance time series, is given by Love and Gannon [2009, Figure 12]. The cause of the asymmetry is a combination of forces due to magnetic field gradients and convective electric fields. This results in a concentration (reduction) of ion drift lines of trajectory in the dusk (dawn) magnetosphere [e.g., Takahashi *et al.*, 1990; Liemohn *et al.*, 2001], or, equivalently, a dusk-centered partial ring current.

[36] These observations are not obviously consistent with the standard picture of substorms and associated abrupt collapses of current in the magnetotail [e.g., McPherron, 1991; Kamide *et al.*, 1998b], which should give positive midnight-centered disturbance. Nor are they obviously consistent with various types of satellite data, which tend to show a midnight-centered partial ring current [e.g., Cson Brandt *et al.*, 2002; Le *et al.*, 2004] that would give a negative midnight-centered disturbance. The discrepancy has been explained as a “shielding effect” related to field-aligned currents [Harel *et al.*, 1981; Crooker and Siscoe, 1981; Wolf *et al.*, 2007], but additional investigation is worthwhile.

[37] Dawn-dusk asymmetry in low-latitude magnetic disturbance is seen during the November 2003 storm (Figure 5) and during the October 2003 storm (Figure 6d). In contrast, the great storm of March 2001 shows a pattern of negative magnetic disturbance that is greatest (least) at midnight (noon) local time [Skoug *et al.*, 2003]. This is unusual. The overwhelming pattern seen in the movie-maps is one of dawn-dusk asymmetry. To emphasize this fact, in Figure 11 we show Dst time series, contour plots of magnetic disturbance, $Dist(\theta_m)$ from equation (8), and the asymmetric component of magnetic disturbance, $Asym(\theta_m) = Dist(\theta_m) - Dst$, over the local time and universal time domains. In (a–c) for the Halloween storm, in (d–f) for three medium-size storms that occurred in quick succession in July 2004, and in (g–i) for the November 2004 storm. In each of these cases, and in most other cases for storms of various sizes, dawn-dusk asymmetry is prominent during storm main phase; relative symmetry is seen during most periods of storm recovery.

6.7. Geographically Fixed Asymmetry

[38] In Figure 11c, days 303.5–304.0 (see, also, movie-map 2003:10:30), a transient asymmetry that is roughly fixed in geographic coordinates is seen (diagonal features in the contour plot). Similar transient asymmetry is seen, for example, in the work by Clauer and McPherron [1974, Figure 2] and in the work by Clauer [2006, Figure 2], although those authors do not comment upon the phenomenon. We suspect that this asymmetry is caused by the tilt of the geomagnetic dipole relative to the Earth’s rotational axis, causing a diurnal modulation in storm time magnetic disturbance. As such, geographically fixed asymmetry might be a manifestation of the well-known semiannual diurnal variation, explained by either the Russell-McPherron [1973] hypothesis or the equinoctial [Bartels, 1925] hypothesis. Again, additional investigation is certainly worthwhile.

6.8. Day the Solar Wind Disappeared

[39] The days of 10–11 May 1999 saw the solar wind pressure, as measured by the ACE satellite, drop to anomalously low levels (~ 0.01 nPa) [Smith *et al.*, 2001]. Not surprisingly, global magnetic conditions were very quiet; the K_p index briefly dropped to 0. This unusual period of time serves as a test of our algorithms for isolating magnetic disturbance and estimating a stable baseline against which disturbance is measured. The movie-map (1999:05.11) includes a 3 day duration of magnetic quiescence, during which time very little happens. Indeed, the most interesting thing about this movie-map is that it is boring. The final day of the movie-map, however, records a small storm, and that is about as exciting as this movie-map gets. We can confidently say that features seen in the other movie-maps recording magnetic storms are not artifacts of unremoved solar quiet variation.

7. Conclusion

[40] In constructing our movie-maps, we have become very well acquainted with some of the time-dependent evolutionary details of individual storms. And we recognize that the movie-maps contain so much information that it is impossible to summarize it all at once. As always, there is much that remains to be done. We plan on investigating a similar movie-map display of magnetic observatory declination data, which should reveal patterns in field-aligned currents. In the mean time, our hope is that the movie-maps of horizontal-intensity disturbance presented here will be useful for other research scientists.

[41] Acknowledgments. We thank the many institutes listed in Table 1 for their support of magnetic observatory operations. We acknowledge INTERMAGNET (www.intermagnet.org) for its role in promoting high standards of magnetic observatory practice. We thank the ACE, GEOTAIL, WIND, and GOES science centers for collecting solar wind and interplanetary magnetic field data; we thank NASA’s OmniWeb and CDAWeb teams for making data easily available. We thank W. J. Burke, J. E. Caldwell, C. A. Finn,

J. P. McCollough, and two anonymous referees for reviewing a draft manuscript. We thank C. R. Clauer, J. C. Green, T. Iyemori, R. L. McPherron, K. Mursula, T. G. Onsager, H. J. Singer, B. T. Tsurutani, and G. R. Wilson for useful conversations. The USGS Geomagnetism Program has supported this work, the present operation of the Honolulu, San Juan, Stennis, and Tucson observatories, and the past operation of the Del Rio and Midway observatories.

References

- Akasofu, S. I., and S. Chapman (1972), *Solar-Terrestrial Physics*, Oxford Univ. Press, Oxford, U. K.
- Baker, D. N., et al. (2009), *Severe Space Weather Events: Understanding Societal and Economic Impacts*, Natl. Acad. Press, Washington, D. C.
- Balch, C., B. Murtagh, D. Zezula, L. Combs, G. Nelson, K. Tegnell, M. Crown, and B. McGehan (2004), Intense space weather storms October 19–November 07, 2003, service assessment, NOAA, U.S. Dep. of Commerce, Silver Spring, Md.
- Bartels, J. (1925), Eine universelle Tagesperiode der erdmagnetischen Aktivität, *Meteorol. Z.*, 42, 147–152.
- Chapman, S., and J. Bartels (1962), *Geomagnetism*, Oxford Univ. Press, London.
- Chapman, S., and V. C. A. Ferraro (1930), A new theory of magnetic storms, *Nature*, 126, 129–130.
- Clauer, C. R. (2006), The geomagnetic storm-time response to different solar wind driving conditions, in *The Solar Influence on the Heliosphere and Earth's Environment: Recent Progress and Prospects—Proceedings of the ILWS Workshop*, edited by N. Gopalswamy and A. Bhattacharyya, pp. 332–339, Quest, Birmingham, Ala.
- Clauer, C. R., and R. L. McPherron (1974), Mapping local time–universal time development of magnetospheric substorms using mid-latitude magnetic observations, *J. Geophys. Res.*, 79, 2811–2820.
- Clauer, C. R., I. I. Alexeev, E. S. Belenkaya, and J. B. Baker (2001), Special features of the September 24–27, 1998 storm during high solar wind dynamic pressure and northward interplanetary magnetic field, *J. Geophys. Res.*, 106, 25,695–25,711.
- Clauer, C. R., M. W. Liemohn, J. U. Kozyra, and M. L. Reno (2003), The relationship of storms and substorms determined from mid-latitude ground-based magnetic maps, in *Disturbances in Geospace: The Storm-Substorm Relationship*, *Geophys. Monogr. Ser.*, vol. 142, edited by A. S. Sharma, Y. Kamide, and G. S. Lakhina, pp. 143–157, AGU, Washington, D. C.
- Cowley, S. W. H. (1995), The Earth's magnetosphere: A brief beginner's guide, *Eos Trans. AGU*, 76(51), 525.
- Crooker, N. U., and G. L. Siscoe (1981), Birkeland currents as the cause of the low-latitude asymmetric disturbance field, *J. Geophys. Res.*, 86, 11,201–11,210.
- Cson Brandt, P., S. Ohtani, D. G. Mitchell, M.-C. Fok, E. C. Roelof, and R. Demajistre (2002), Global ENA observations of the storm mainphase ring current: Implications for skewed electric fields in the inner magnetosphere, *Geophys. Res. Lett.*, 29(20), 1954, doi:10.1029/2002GL015160.
- Cummings, W. D. (1966), Asymmetric ring currents and the low-latitude disturbance daily variation, *J. Geophys. Res.*, 71, 4495–4503.
- Daglis, I. A., R. M. Thorne, W. Baumjohann, and S. Orsini (1999), The terrestrial ring current: Origin, formation, and decay, *Rev. Geophys.*, 37, 407–438.
- Dessler, A. J., and E. N. Parker (1959), Hydromagnetic theory of geomagnetic storms, *J. Geophys. Res.*, 64, 2239–2252.
- Dungey, J. W. (1961), Interplanetary magnetic field and the auroral zones, *Phys. Rev. Lett.*, 6, 47–48.
- Fukushima, N., and Y. Kamide (1973), Partial ring current models for worldwide geomagnetic disturbances, *Rev. Geophys.*, 11, 795–853.
- Gannon, J. L., and J. J. Love (2010), USGS 1-min Dst index, *J. Atmos. Sol. Terr. Phys.*, in press.
- Gonzalez, W. D., J. A. Joselyn, Y. Kamide, H. W. Kroehl, G. Rostoker, B. T. Tsurutani, and V. M. Vasiliunas (1994), What is a geomagnetic storm?, *J. Geophys. Res.*, 99, 5771–5792.
- Gopalswamy, N., L. Barbieri, E. W. Cliver, G. Lu, S. P. Plunkett, and R. M. Skoug (2005), Introduction to violent Sun-Earth connection events of October–November 2003, *J. Geophys. Res.*, 110, A09S00, doi:10.1029/2005JA011268.
- Harel, M., R. A. Wolf, R. W. Spiro, P. H. Reiff, C. K. Chen, W. J. Burke, F. J. Rich, and M. Smiddy (1981), Quantitative simulation of a magnetospheric substorm: 2. Comparison with observations, *J. Geophys. Res.*, 86, 2242–2260.
- Jankowski, J., and C. Sucksdorff (1996), *Guide for Magnetic Measurements and Observatory Practice*, Int. Assoc. of Geomagn. and Aeron., Warsaw.
- Kamide, Y., N. Yokoyama, W. Gonzalez, B. T. Tsurutani, I. A. Daglis, A. Brekke, and S. Masuda (1998a), Two-step development of geomagnetic storms, *J. Geophys. Res.*, 103, 6917–6921.
- Kamide, Y., et al. (1998b), Current understanding of magnetic storms: Storm–substorm relationships, *J. Geophys. Res.*, 103, 17,705–17,728.
- Kennel, C. F. (1995), *Convection and Substorms: Paradigms of Magnetospheric Phenomenology*, Oxford Univ. Press, Oxford, U. K.
- Kerridge, D. J. (2001), INTERMAGNET: Worldwide near realtime geomagnetic observatory data, paper presented at ESA Space Weather Workshop, Eur. Space Res. and Technol. Cent., Noordwijk, Netherlands. (Available at <http://www.esa-spaceweather.net/spweather/workshops/workshops.html>.)
- Kozyra, J. U., and M. W. Liemohn (2003), Ring current energy input and decay, *Space Sci. Rev.*, 109, 105–131.
- Le, G., C. T. Russell, and K. Takahashi (2004), Morphology of the ring current derived from magnetic field observations, *Ann. Geophys.*, 22, 1267–1295, sref:1432-0576/ag/2004-22-1267.
- Liemohn, M. W., J. U. Kozyra, M. F. Thomsen, J. L. Roeder, G. Lu, J. E. Borovsky, and T. E. Cayton (2001), Dominant role of the asymmetric ring current in producing the stormtime Dst*, *J. Geophys. Res.*, 106, 10,883–10,904.
- Love, J. J. (2008), Magnetic monitoring of Earth and space, *Phys. Today*, 61, 31–37.
- Love, J. J., and J. L. Gannon (2009), Revised Dst and the epicycles of magnetic disturbance: 1958–2007, *Ann. Geophys.*, 27, 3101–3131.
- McPherron, R. L. (1991), Physical processes producing magnetospheric substorms and magnetic storms, in *Geomagnetism*, vol. 4, edited by J. A. Jacobs, pp. 593–739, Academic, London.
- McPherron, R. L. (1997), The role of substorms in the generation of magnetic storms, in *Magnetic Storms*, *Geophys. Monogr. Ser.*, vol. 98, edited by B. T. Tsurutani et al., pp. 131–147, AGU, Washington, D. C.
- Moos, N. A. F. (1910a), *Colaba Magnetic Data, 1846 to 1905: Part I—Magnetic Data and Instruments*, Gov. Cent. Press, Bombay, India.
- Moos, N. A. F. (1910b), *Colaba Magnetic Data, 1846 to 1905: Part II—The Phenomenon and its Discussion*, Gov. Cent. Press, Bombay, India.
- Nishida, A. (1994), Foward of GEOTAIL special issue, *J. Geomagn. Geoelectr.*, 46, 3–5.
- Panasyuk, M. I., et al. (2004), Magnetic storms in October 2003, *Cosmic Res.*, 42, 489–534.
- Potapov, A., A. Guglielmi, B. Tsegmed, and J. Kultima (2006), Global PC5 event during 29–31 October 2003 magnetic storm, *Adv. Space Res.*, 38, 1582–1586.
- Prölls, G. W. (2004), *Physics of the Earth's Space Environment*, Springer, Berlin.
- Rasson, J. L. (2007), INTERMAGNET, in *Encyclopedia of Geomagnetism and Paleomagnetism*, edited by D. Gubbins and E. Herrero-Bervera, pp. 715–717, Springer, New York.
- Rostoker, G., and C. G. Fälthammar (1967), Relationship between changes in the interplanetary magnetic field and variations in the magnetic field at the Earth's surface, *J. Geophys. Res.*, 72, 5853–5863.
- Russell, C. T. (1995), Foward of WIND special issue, *Space Sci. Rev.*, 71, 1–4.
- Russell, C. T., and R. L. McPherron (1973), Semiannual variation of geomagnetic activity, *J. Geophys. Res.*, 78, 92–108.
- Russell, C. T., R. L. McPherron, and R. K. Burton (1974), On the cause of geomagnetic storms, *J. Geophys. Res.*, 79, 1105–1109.
- Russell, C. T., M. Ginskey, S. Petrinec, and G. Le (1992), The effect of solar wind dynamic pressure changes on low and mid-latitude magnetic records, *Geophys. Res. Lett.*, 19, 1227–1230.
- Sabine, E. (1856), On periodical laws discoverable in the mean effects of the larger magnetic disturbances. No. III, *Philos. Trans. R. Soc. London*, 146, 357–374.
- Sckopke, N. (1966), A general relation between the energy of trapped particles and the disturbance field over the Earth, *J. Geophys. Res.*, 71, 3125–3130.
- Shi, Y., E. Zesta, L. R. Lyons, A. Boudouridis, K. Yumoto, and K. Kitamura (2005), Effect of solar wind pressure enhancements

- on storm time ring current asymmetry, *J. Geophys. Res.*, 110, A10205, doi:10.1029/2005JA011019.
- Singer, H., L. Matheson, R. Grubb, A. Newman, and D. Bouwer (1996), Monitoring space weather with the GOES magnetometers, in *GOES-8 and Beyond*, vol. 2812, edited by E. R. Washwell, pp. 299–308, Soc. of Photo-Optical Instrum. Eng., Bellingham, Wash.
- Singer, S. F. (1957), A new model of magnetic storms and aurorae, *Eos Trans. AGU*, 38, 175–190.
- Siscoe, G. L. (2006), Global force balance of region 1 current system, *J. Atmos. Sol. Terr. Phys.*, 68, 2119–2126.
- Skoug, R. M., et al. (2003), Tail-dominated storm main phase: 31 March 2001, *J. Geophys. Res.*, 108(A6), 1259, doi:10.1029/2002JA009705.
- Skoug, R. M., J. T. Gosling, J. T. Steinberg, D. J. McComas, C. W. Smith, N. F. Ness, Q. Hu, and L. F. Burlaga (2004), Extremely high speed solar wind: 29–30 October 2003, *J. Geophys. Res.*, 109, A09102, doi:10.1029/2004JA010494.
- Smith, C. W., D. J. Mullan, N. F. Ness, R. M. Skoug, and J. Steinberg (2001), Day the solar wind almost disappeared: Magnetic field fluctuations, wave refraction and dissipation, *J. Geophys. Res.*, 106, 18,625–18,634.
- Søraas, F., M. Sørbo, K. Aarsnes, and D. S. Evans (2006), Ring current behavior inferred from ground magnetic and space observations, in *Recurrent Magnetic Storms: Corotating Solar Wind Streams*, *Geophys. Monogr. Ser.*, vol. 167, edited by B. T. Tsurutani et al., pp. 85–95, AGU, Washington, D. C.
- Stone, E. C., A. M. Frandsen, R. A. Mewaldt, E. R. Christian, D. Margolies, J. F. Ormes, and F. Snow (1999), The Advanced Composition Explorer, *Space Sci. Rev.*, 86, 1–22.
- Sugiura, M. (1964), Hourly values of equatorial Dst for the IGY, *Ann. Int. Geophys. Year*, 35, 9–45.
- Sugiura, M., and T. Kamei (1991), Equatorial Dst index 1957–1986, *IAGA Bull.* 40, Int. Serv. Geomagn. Indices Publ. Off., Saint-Maur-des-Fossés, France.
- Takahashi, S., T. Iyemori, and M. Takeda (1990), A simulation of the storm-time ring current, *Planet. Space Sci.*, 38, 1133–1141.
- Wolf, R. A., R. W. Spiro, S. Sazykin, and F. R. Toffoletto (2007), How the Earth's inner magnetosphere works: An evolving picture, *J. Atmos. Sol. Terr. Phys.*, 69, 288–302.
- Zaitzev, A. N., and R. Boström (1971), On methods of graphical displaying of polar magnetic disturbances, *Planet. Space Sci.*, 19, 643–649.

J. L. Gannon and J. J. Love, Geomagnetism Program, U.S. Geological Survey, Box 25046, MS 966, DFC, Denver, CO 80225, USA. (jlove@usgs.gov)